Health, demographic change and wellbeing
Personalising health and care: Advancing active and healthy ageing
H2020-PHC-19-2014
Research and Innovation Action

Deliverable D6.4

Algorithms for cutaneous feedback and wearable haptics

Deliverable due date: 04/2017	**Actual submission date: 30/05/2017**
Start date of project: February 1, 2015	**Duration: 42 months**
Lead beneficiary for this deliverable: UNISI	**Revision: —-**
Authors: Tommaso Lisini Baldi (UNISI), Marco Aggravi (UNISI), Domenico Prattichizzo (UNISI)	
Internal reviewer: Antonis Argyros (FORTH)	

The research leading to these results has received funding from the European Union's H2020 Research and Innovation Programme - Societal Challenge 1 (DG CONNECT/H) under grant agreement n° 643644.

Dissemination Level		
PU	Public	**X**
CO	Confidential, only for members of the consortium (including the Commission Services)	

Contents

Deliverable Summary

The deliverable D6.4 comprises the final release of methods and algorithms in charge of generating and displaying cutaneous feedback to guide humans. Contextually the deliverable deals with the final release of wearable haptic devices for social interaction. The deliverable is related to the Milestone Ms9, due at M27.
Concerning the algorithms to generate cutaneous stimuli, two tasks were devoted to evaluate methodologies and strategies to provide haptic cues to the user.
Task T6.2 "Methods and algorithms to provide haptic information" was focused on studying and producing haptic interaction paradigms to inform the user about direction to follow, positions to reach, and cadence to sync. At the same time of T6.2, task T6.3 "Design of wearable haptic devices for social activities interaction" was in charge of providing social activities interaction by means of novel wearable haptic interfaces, which are thought to be connected to the CPSN.
Three were the required outputs of T6.2 and T6.3:
(*i*) Human-human formation;
(*ii*) Social running and social walking;
(*iii*) Body limb guidance.
The former study evaluated the usability of the wearable haptic interface to guide single or multiple humans towards predefined goals. Algorithms originally developed for robots have been enhanced, taking into account limitations and characteristics of the non-holonomic human model. More in details, Rapidly-exploring Random Tree (RRT), Reciprocal Velocity Obstacle (RVO), and Optimal Reciprocal Collision Avoidance (ORCA) have been tested. These algorithms are able to suggest, through two haptic armbands, the three basic human walking behaviours: turn left, turn right, and go straight. The second output was focused on suggesting pace and linear velocity to the user using two haptic anklets following hints suggested by the CPSN. The latter was about guiding specific part of the body in movements and exercise.
Task T6.2 and T6.3 started with the project at M1 and ended at M27.

Whereas task T6.2 deals with "how to inform" the users with novel haptic paradigms, task T6.3 is in charge of actually provide such cues to the users in "meaningful" ways, so that the user requirements and control directives from WP1 and WP2 are respected.
Concerning the human interface, a visual feedback regarding direction and navigation is provided to the FriWalk users. This visual interface is also the primary means for providing input to the system, by selecting destinations and modes of operation. The video interface has been designed for emphasizing the easiness and the simplicity of use, taking into account the class of potential users. In particular, the visual interface should not distract the user by capturing her/his attention beyond what is required for the interaction. Further developments of the visual interfaces are due inside task T6.4 "FriWalk construction and FriTab interfaces: design and testing", where the prototype is constructed and tested. In fact, this task starts at M10, thus the human interface here described is result of the previous developments brought forward on the FriWalk.
In what follows, we describe how the tasks characteristics were addressed. Chapter 1 presents all the steps and intermediate targets achieved to reach the final goal. Three different guidance algorithms using haptic feedback are described in detail. Chapter 2 deals with cutaneous pinching techniques for user arm rotational guidance.

Chapter 3 depicts the paradigm defined for providing users of a CPSN with walking/running pace of one or other users of the same CPSN, the so-called “social running”. The last part of this deliverable briefly, identified with Chapter 4, describes the principles that have driven the design of the interface, and give examples of the mode of interaction.

Chapter 1

Evaluation of gudiance algorithms using haptic feedback

Workpackage 6 is in charge of the development of the FriWalk, and of the implementation of its additional functionalities. It includes Task T6.2 which outcome was the developments of methods and algorithms to provide haptic information, and Task T6.3 that aimed to design a novel wearable haptic devices and study paradigms for social activities interactions. In this chapter we summarize and detail all the steps for the complete guidance algorithm. Firstly, we evaluated the capability of a user to follow haptics cues, then we describe a strategy to guide humans along a predefined path. Finally we present the extension of the previous algorithm to guide people without the FriWalk towards a goal, suggested by the CPSN, in a collision-free path in dynamic environment.
The steering guidance aglorithms developed and the implementation of the human-human formation are technological pillars of T6.2 and T6.3, respectively. The results here presented have been included in international conferences proceedings [1, 54], [56] and part are still preliminary and/or submitted to international conferences and journals.

1.1 Introduction

In real world scenarios, visual and auditory channels may be overloaded with information, thus resulting in a rapid error increase and in an overall user performance reduction if directional cues are provided through these channels. A possible solution is to deliver this information exploiting an underutilized sense, i.e., the sense of touch. As with sound, a tactile stimulus is made up of a signal with varying frequency and amplitude, but different from the auditory feedback, tactile feedback directly engages our motor learning system [37] with extraordinary sensitivity and speed [26]. Moreover, tactile communication can be used in situations where visual or auditory stimuli are distracting, impractical, unavailable or unsafe. Possible scenarios consist in helping a person who is in a dangerous situation or guiding a person toward a point of interest. In the case of the ACANTO project this represents a real need. Let us consider one or multiple users, walking with the FriWalk or with the FriTab. The user would be suggested by the CPSN of possible locations or friends to visit. In our approach, subjects are free to select their desired linear velocity, i.e., the walking speed, while control signals are sent for steering the locomotions, i.e., the direction. Moreover, the person always remains in charge of the final decision to take, the type of correction provided to the user should be perceived as very soft, and unnatural stimulations must be avoided as much as possible.
Recently Arechavaleta *et al.* [3] has shown a close relationship between the shape of human locomotor paths in goal-directed movements and the simplified kinematic model of a wheeled mobile robot. Thus, nonholonomic constraints similar to those of mobile robots are used for describing the human walking. In addition, this

assumption meets the constraints induced when the user is walking with the help of the FriWalk. These results provided us with the theoretical ground for adapting control strategies developed for unicycle robots, to human subjects.
Vibrotactile haptic guidance has been successfully exploited in the last years. Closely related are the researches presented in [68, 38, 9], and [54]. In [68], a vibrotactile belt is used for waypoint navigation in an outdoor environment. A torso-mounted vibrotactile display was used in [38] to provide vibrotactile cues for improving the situational awareness of soldiers in a simulated building-clearing exercise. A vibrotactile belt was used in [9] where the authors presented a navigation guidance system that guides a human to a goal point. Differently from the aforementioned works, they modeled the human as a nonholonomic robot and showed that control algorithms used for mobile robots can be opportunely translated to human guidance scenarios. Strictly related is a work of Scheggi *et. al* [54], where the authors presented a new paradigm for the assisted navigation of mixed human-robot teams using haptic information. Finally in [32], the authors proposed a mobile device for human navigation using multimodal communication (audio, visual, vibrotactile and directional skin-stretch stimuli). In [3], authors show that non-holonomic constraints can approximate the human walking. In particular, they claim that the human locomotion can be approximated by the motion of a unicycle system. In our approaches, we model the human locomotion as a unicycle system. In what follows we present two different haptic guidance policies studied and developed to steer the human towards a predefined goal.

1.2 Human Navigation using haptic stimuli

We start this document proposing a novel use of haptic feedback for human navigation. We tested this approach in a robot-assisting navigation. Assuming that a human wants to reach a final location in a large environment with the help of a mobile robot, the robot must steer the human from the initial to the target position. The challenges posed by cooperative human-robot navigation are typically addressed by using kinesthetic haptic feedback via physical interaction.
By contrast, we here describe a different approach in which the human-robot interaction is achieved via wearable vibrotactile devices. Different from related approaches, in the proposed work the subject is free to decide her/his own pace and a warning vibrational signal is generated by the haptic bracelets only when a large deviation with respect to the desired pose is detected by the robot. The proposed method has been evaluated in a large indoor environment where fifteen blindfolded human subjects were asked to follow the haptic cues provided by the robot in order to reach a target area, while avoiding static and dynamic obstacles. Experimental results revealed that the blindfolded subjects were able to avoid the obstacles and safely reach the target in all the performed trials. A comparison is provided between the results obtained using this approach with blindfolded users and experiments performed with sighted people.

1.2.1 Introduction

This preliminary study presents a novel use of haptic feedback for guiding human in cooperative human-robot navigation scenario. Let us assume that a human wants to reach a final location in a large environment with the help of a mobile robot (see Fig. 1.1). Possible scenarios consist in: (i) assisting an older adult or a visually-impaired person; (ii) helping a person who is in a dangerous situation with poor visibility and no way of hearing clearly due to environmental noise. We started from the real needs raised within the ACANTO project. Examples are an exercise suggested by the FriTab, or a destination proposed through the CPSN. In our approach, the human is free to select her/his desired linear velocity and the robot does not force her/him to its pace as long as environmental obstacles are avoided and she/he is able to safely reach the target location. The robot, that can be easily replaced by the FriWalk, guides the human by only adjusting her/his angular velocity, in a way that the person always remains in charge of the final decision to take, and she/he can always override the

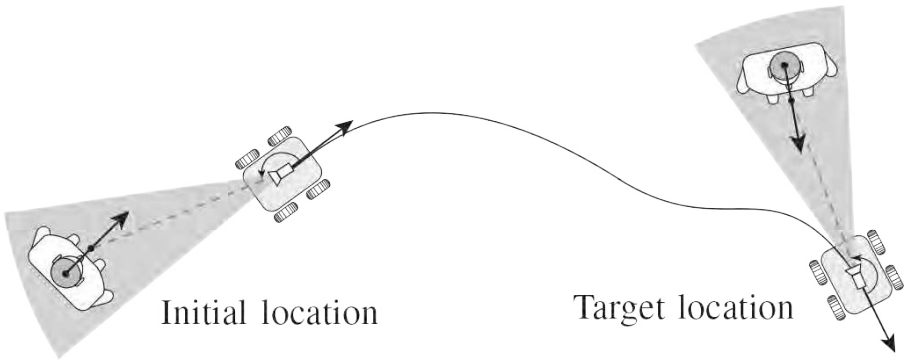

Figure 1.1: Cooperative human-robot navigation from an initial to a target location (top view). The goal is to guide a human in a large environment with the help of a mobile robot. The interaction between the user and the robot is obtained via wearable haptic interfaces which provide the user with directional cues in order to reach the target, while avoiding static and dynamic obstacles. The robot and the human are respectively equipped with a *vision sensor* and wrist-worn *vibrotactile bracelets*. The field of view of the vision sensor (an RGB-D camera in this study) is shaded.

"suggestions" given by the system. The type of correction provided by the robot has to be perceived as very *soft*, and unnatural stimulations must be avoided as much as possible.

We used haptic signals provided by cutaneous devices in order to correct the human's angular velocity. The main source of inspiration for this chapter came from [17], where a passive approach inspired by the classical "Cobot" philosophy [44] is adopted for guiding an elderly person using the brakes of a commercial walker, and from [11] where the authors propose a leader-follower formation control strategy, which has been adapted to our peculiar human-robot setup. Strictly related to our work is the study presented in [22] where the authors investigated the design of a stiff rein which could enhance human trust and confidence in cooperative human-robot tasks. Their final design consists in a stiff handle attached to the robot via a mechanical feedback spring system at the base. When the user is aligned with the robot, the spring system has zero tension. When the handle is being rotated, the spring system introduces tension on the handle, which increases with the rotation angle. In [19], the authors developed an assistive-guide prototype robot to help visually-impaired people to navigate unfamiliar areas. The human-robot interaction is achieved using a leash and the robot control does not take into account the user's motion but only the deviation of the robot from the reference path or the proximity from obstacles. Moreover, the authors did not focus on how the human interacts with the robot. In [50, 49], the authors presented identifications of human-human interactions via a hard rein along a given path. The derived interaction model can be used to design a robot-human guidance for helping people move in dangerous situations were they can not use their main sensory modalities. While kinesthetic feedback is common in haptic systems, we used vibrotactile interfaces since tactile devices are generally more portable, less encumbering and have a wider range of action than the kinesthetic ones [39]. Different from the works mentioned above, our approach does not require physical interaction between the human and the robot. In fact, although using a hard rein or a stiff handle is very effective in terms of tactile stimuli and can guide the human subject in a more effective way than vibrotactile stimuli, we consider the physical interaction limiting: (i) the user has her/his hands busy, thus other physical tasks may not be accomplishable; (ii) it is difficult to extended the physical interaction to multiple users; (iii) since we are using wearable devices, the proposed approach can be extended to other body parts, for example it can be combined/extended to guide the arms of the user along feasible trajectories in cooperative manipulation/transportation tasks. Different from [22, 19], we designed a control policy such that the robot adjusts its linear velocity according to the human's one.

Haptic feedback for human guidance have been used in [4], where the authors used a grounded haptic manipu-

lator to apply kinesthetic force and position signals to the user's hand in order to assist the operator in reaching a desired position in large remote environments.
Wearable haptic devices were used in [15], where an haptic belt was used for waypoint navigation. The system relied not only on vibrotactile stimuli but also on GPS information which is not available in indoor or some outdoor environments. A similar approach was used in [10] where the authors presented a navigation guidance system that guides a human to a goal point with a tactile belt interface. Similarly to our work, they modeled the human as a nonholonomic robot, however they used a different way to provide vibrotactile stimuli to the user, they did not considered haptic stimuli for human-robot cooperative navigation and they did not present a human-robot formation control algorithms.
Finally in [32], the authors proposed a mobile device for human navigation using multimodal communication (audio, visual, vibrotactile and directional skin-stretch stimuli).
For human-robot cooperation, recent studies have proved the importance of haptic feedback for role negotiation in human-robot co-manipulation tasks (cf. [13, 60]). Similarly, in [63] the authors proposed an approach that exploit the arm compliance of a humanoid robot to follow the human guidance in a physical human-robot cooperative task.

1.2.2 Original contributions and organization

Our setup consists of a mobile robot equipped with a vision sensor (an RGB-D camera, like the one embedded in the FriWalk) and a human subject wearing custom-design vibrotactile interfaces. We assume that the robot has a map of the environment. The robot can autonomously localize its pose in the map and guide the user along obstacle-free paths. Obstacle-free paths are computed for both the robot and the user and updated as soon as new obstacles are detected by the robot. Since a predefined distance and orientation should be maintained between the human and the robot at all times, the leader-follower formation control strategy proposed in [11] has been adapted to our human-robot setup.
In fact, recent studies [3] have shown a close relationship between the shape of human locomotor paths in goal-directed movements, and the simplified kinematic model of a wheeled mobile robot. In particular, the authors have shown that the shoulders can be considered as a sort of steering wheel that drives the human body with a short delay. From a kinematic perspective, this observation indicates that humans move tangentially to their walking trajectory, i.e. the direction of their body is tangent to the trajectories they perform. Different from [11], in our scenario the human should always be able to freely select her/his linear velocity. However, a specific haptic feedback is sent to the user in order to adjust her/his angular velocity according to the formation specifics. Our purpose is to send easily processable signals to the human (by exploiting the nonholonomic constraints of her/his walking motion), so that she/he can promptly respond to the stimuli of the guiding robot.

1.2.3 Problem formulation and control design

We review the leader-follower formation control strategy proposed in [11], and show how to adapt it to our human guidance setup. Nonholonomic constraints, similar to those describing the motion of a unicycle robot, seem to be at work when a human is walking [3], leader-follower formation control can also be applied (with suitable modifications) to a mixed human-robot formation (cf. [57, 54]).
The robots are considered as velocity-controlled nonholonomic platforms with two independent inputs. Let us consider a robot whose kinematics can be abstracted as a unicycle model,

$$\dot{x} = v\cos\theta, \qquad \dot{y} = v\sin\theta, \qquad \dot{\theta} = \omega, \tag{1.1}$$

where $\mathbf{R} = (x,\, y,\, \theta)^T \in \mathbb{R}^2 \times \mathbb{S}^1$ is the pose of the robot, $\overline{\mathbf{R}} = (\overline{x},\, \overline{y},\, \overline{\theta})^T$ is the initial position and heading, and $(v,\, \omega)^T$ is the control input. We denote by $\mathbf{P} = (x,\, y)^T$ the position of the robot.

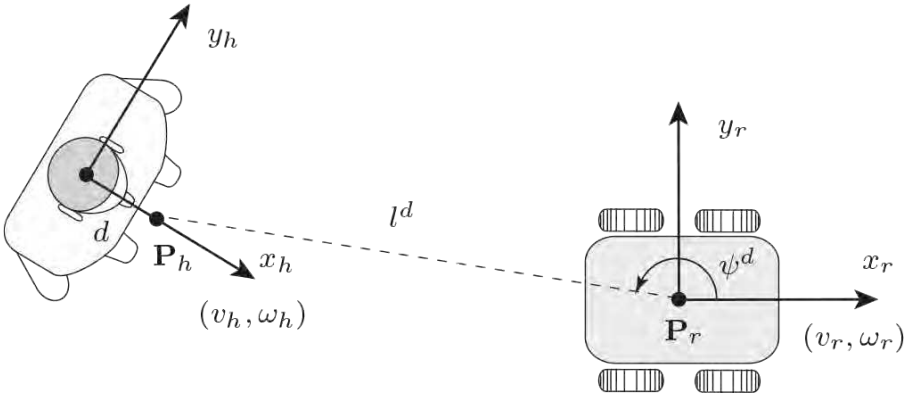

Figure 1.2: Human-robot setup: l^d and ψ^d represent the desired distance and orientation between the robot and an off-axis reference point $\mathbf{P}_h$ on the human with offset d. The human and the robot move with linear and angular velocity (v_h, ω_h) and (v_r, ω_r), respectively.

With these definitions at hand, let us now briefly review the leader-follower setup proposed in [11]. Here, robot $\mathbf{R}_h$ (in our framework, a *human*) must follow the robot $\mathbf{R}_r$ with a desired separation l^d and desired relative bearing ψ^d (see Fig. 1.2). In what follows, subscripts h and r refer to the human and to the robot, respectively. Note that ψ^d describes the heading direction of the human with respect to the robot. Let $\beta = \theta_r - \theta_h$ be the relative orientation of $\mathbf{R}_h$ and $\mathbf{R}_r$, $\mathbf{u}_r = (v_r,\, \omega_r)^T$ and $\mathbf{u}_h = (v_h,\, \omega_h)^T$ their control inputs, and

$$\mathbf{G} = \begin{bmatrix} \cos\gamma & d\sin\gamma \\ \frac{-\sin\gamma}{l} & \frac{d\cos\gamma}{l} \end{bmatrix}, \quad \mathbf{F} = \begin{bmatrix} -\cos\psi & 0 \\ \frac{\sin\psi}{l} & -1 \end{bmatrix},$$

where d is the offset to an off-axis reference point $\mathbf{P}_h$ on $\mathbf{R}_h$, $\gamma = \beta + \psi$ and l, ψ are the separation and relative bearing of $\mathbf{R}_h$ and $\mathbf{R}_r$, respectively (see Fig. 1.2). The control input for $\mathbf{R}_h$ can then be written as,

$$\mathbf{u}_h = \mathbf{G}^{-1}(\mathbf{q} - \mathbf{F}\,\mathbf{u}_r), \tag{1.2}$$

being $\mathbf{q}$ an auxiliary control input defined as

$$\mathbf{q} = \begin{bmatrix} k_1(l^d - l) \\ k_2(\psi^d - \psi) \end{bmatrix}, \tag{1.3}$$

where k_1, k_2 are positive control gains (observe that $\mathbf{G}$ is always invertible as long as $d/l > 0$, which always holds true). Eq. (1.2) has been obtained by applying input-output linearization (see [62]).
In what follows, we will show how to tailor (1.2) to our human-guidance problem. Notice that in our framework the distinction between leader and follower vanishes: in fact, here both agents cooperate to achieve a common goal (reach the desired target), without direct physical interaction.

1.2.4 Human-robot guidance

Different from [11], in our scenario the human should always be able to freely choose her/his linear velocity. However, in order to be driven by the robot $\mathbf{R}_r$ toward a target position, her/his angular velocity should be suitably regulated. On the other side, the robot should change its linear velocity accordingly to that of the user, while its angular velocity depends on the specific trajectory from the initial to the target position. Since the desired geometric path of the robot is the result of an on-board planning algorithm, we assume the trajectory

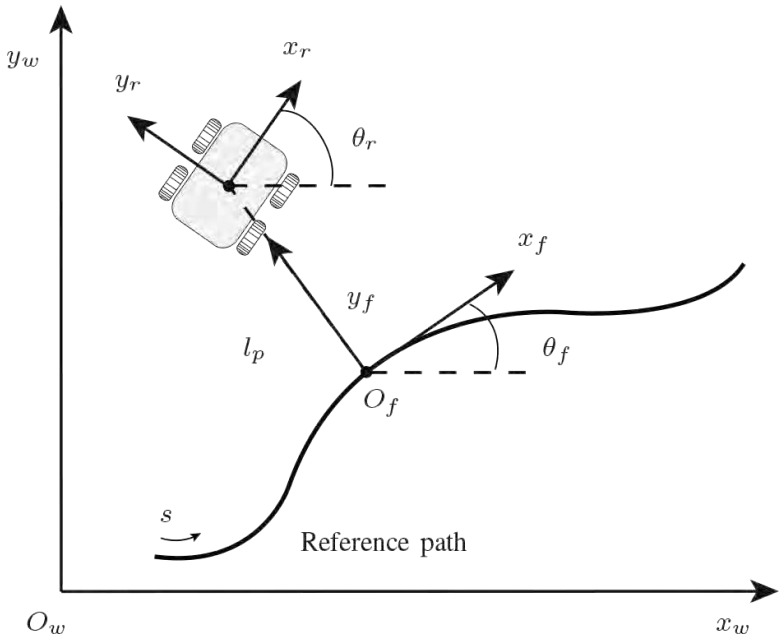

Figure 1.3: Path following setup: l_p represents the coordinate of the vehicle position along the y-axis of the Frenet frame $\langle O_f, x_f, y_f \rangle$, s is the curvilinear coordinate of the robot along the path, θ_f and θ_r represent the angle between the x-axis of the world frame $\langle O_w, x_w, y_w \rangle$ and the x-axis of the Frenet and robot frame, respectively.

to be smooth (the tangent to the trajectory is well defined at each point), and that its curvature is known at any point. We assume that the vehicle is always localized with respect to the path and that a Frenet frame moving along the path, whose origin is the orthogonal projection of the vehicle position on the path, is always available (see Fig. 1.3). The desired angular velocity ω_r of the robot that solves the path following problem, assuming that the initial robot configuration is not far from the desired path and that $v_r > 0$, is

$$\omega_r = v_r \; a_r, \tag{1.4}$$

being

$$a_r = -k_3 l_p \frac{\sin(\theta_p)}{\theta_p} - k_4 \theta_p + \cos(\theta_p) \frac{c(s)}{1 - c(s) l_p},$$

where k_3, k_4 are positive control gains, l_p represents the signed distance of the vehicle position along the y-axis of the Frenet frame, $\theta_p = \theta_r - \theta_f$, being θ_f the angle between the x-axis of the world frame $\langle O_w, x_w, y_w \rangle$ and the x-axis of the Frenet frame, s is the curvilinear coordinate along the path, and $c(s)$ is the curvature of the path at that point, defined as $c(s) = d\theta_f / ds$ [6].
Concerning the cooperative navigation control law, let

$$\mathbf{G}_f = \begin{bmatrix} d \sin\gamma & -\cos\psi \\ \frac{d\cos\gamma}{l} & \frac{\sin\psi}{l} \end{bmatrix}, \quad \mathbf{F}_f = \begin{bmatrix} \cos\gamma & 0 \\ \frac{-\sin\gamma}{l} & -1 \end{bmatrix},$$

then the control velocities for the human and robot are given by (cf. (1.2)),

$$\begin{bmatrix} \omega_h \\ v_r \end{bmatrix} = (\mathbf{G}_f)^{-1} \Big(\mathbf{q} - \mathbf{F}_f \begin{bmatrix} v_h \\ \omega_r \end{bmatrix} \Big). \tag{1.5}$$

It is worth noting that input-output linearization is possible as long as $\cos(\gamma - \psi) \neq 0$. Assuming that the human is moving with linear velocity v_h and the robot is rotating with angular velocity ω_r, then the control law reported in (1.5) allow to maintain the formation specified by l^d and ψ^d.
Substituting (1.4) in (1.5), we obtain the following human-robot control law which allows the robot to follow a precomputed path,

$$\begin{bmatrix} \omega_h \\ v_r \end{bmatrix} = (\mathbf{G}_{pf})^{-1}(\mathbf{q} - v_h \mathbf{F}_{pf}), \tag{1.6}$$

being

$$\mathbf{G}_{pf} = \begin{bmatrix} d\sin\gamma & -\cos\psi \\ \frac{d\cos\gamma}{l} & \frac{\sin\psi}{l} - a_r \end{bmatrix}, \qquad \mathbf{F}_{pf} = \begin{bmatrix} \cos\gamma \\ \frac{-\sin\gamma}{l} \end{bmatrix}.$$

Observe that $\mathbf{G}_{pf}$ is not invertible if $l^{-1}\cos(\gamma - \psi) - a_r \sin\gamma = 0$ which is equivalent to $\beta = acos(la_r \sin\gamma)$. Suppose that the robot estimates the human motion using an onboard vision sensor with limited field of view (FoV) (cf. Fig. 1.1 and Sec. 1.2.10). Since the formation parameters are fixed with respect to the robot, then a proper choice of l^d and ψ^d allows to maintain the human inside the sensor's field of view. ◇
Note that while it is simple to command a robot with velocity v_r, it is not trivial to impose a desired angular velocity ω_h to a human. In the next section we will show how we can use haptic feedback to address this challenging problem.

1.2.5 Haptic Feedback

In this section, we describe the main features of our haptic device and the nature of the vibrotactile feedback provided to the human. Different from [15, 10], which developed a vibrotactile belt to guide the user. We focused on vibrotactile bracelets, reducing the sites of the vibrating motors in order to elicit only the necessary human's behaviors. Due to the nonholonomic nature of the human locomotion in goal directed path, the device should elicit only three basic behaviors on the human (*turn left*, *turn right*, and *slow down*. As far as the three basic behaviors are concerned, only three stimuli would be sufficient in principle. In order to not overload the tactile channel and to not reduce the recognition time, we decided to display few but significative signals. Thus only three stimuli. Note that, although the human is always free to decide her/his pace, the *slow down* behavior is introduced in case of emergency, danger or when the maximal linear velocity of the robot is not sufficient to keep up the human's velocity.
Providing the user with the best haptic feedback is equal to find a tradeoff between the informativeness, the easiness of use, and the wearability of the haptic devices. In what follows, we present the vibrotactile devices and two haptic cueing methods. The first method, which consists in a more wearable solution, is composed by a single wristband worn on the dominant forearm (*unilateral* condition). The second method, which aims to be more intuitive, used two wristbands placed bilaterally on the forearms (*bilateral* condition). Although the bilateral condition allows a larger spatial separation between the stimuli, and in theory, a better discrimination of the directional cues, the unilateral condition represents a more compact solution.

1.2.6 Description of the haptic bracelet

Tactile vibratory sensitivity is influenced by the spatial location on the body, the distance between the stimulators, the frequency of stimulation and the age of the user. Studies have demonstrated that vibration is best on hairy skin due to skin thickness and nerve depth, and that vibrotactile stimuli are best detected in bony areas [20]. In particular, wrists and spine are generally preferred for detecting vibrations, with arms next in line [31]. Movement can decrease detection rate and increases response time of particular body parts. For example, walking affects lower body sites the most [31]. The effect of movement on vibrotactile sensitivity has been also investigated in [45].

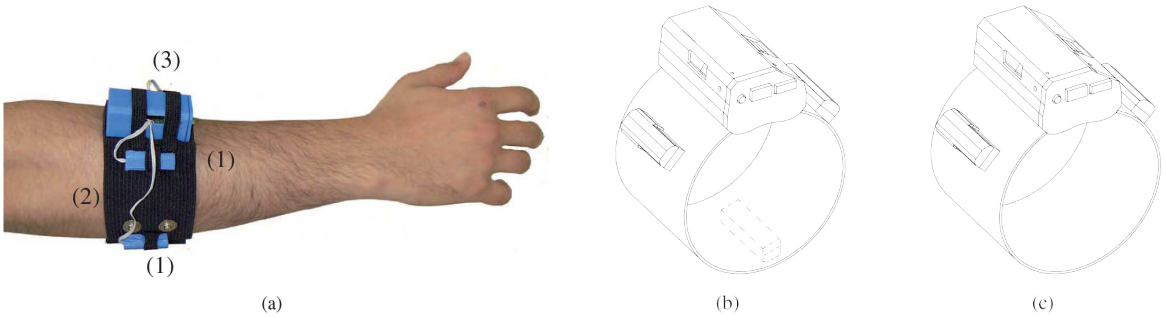

Figure 1.4: (a) The vibrotactile bracelet is fitted on the forearm and it is equipped with vibrating motors (1), attached to an elastic wristband (2) whose width is about 60 mm. The Li-Ion battery and the Arduino board are in (3). Two different configuration were tested: (b) a single bracelet with three vibrating motors; (c) two bracelets with two vibrating motors each.

Due to the aforementioned considerations and since our aim is to design an intuitive and non-obtrusive device which could be easily worn, we concentrated on the development of vibrotactile bracelets. By focusing on a minimal setup composed of a single bracelet (unilateral condition), since the haptic feedback should elicit three basic behaviors, three vibrating motors should be sufficient to independently warn the user. A bracelet shape with three vibrating motors circling the forearm (see Fig. 1.4(a)-(b)) ensures sufficient distance between the motors while covering a minimal forearm area. In fact, the minimal distance between two stimuli to be differentiated is about 35 mm on the forearms: in two point discrimination perception, there is no evidence for differences among the left and right sides of the body and women are known to be more sensitive than men to skin stimulation [70], [20]. In order to improve the *intuitiveness* of the haptic feedback, we investigated a second solution (bilateral condition) in which two haptic bracelets, equipped with two vibrating motors each, are used (see Fig. 1.4(a)-(c)). The subject wears one vibrotactile bracelet on each forearm in order to maximize the stimuli separation while keeping the discrimination process as intuitive as possible. According to [8], in each modality we placed the bracelets close to the elbow in order to maximize the separation between the motors and exert the strongest influence on localization accuracy due to the proximity of stimulus site to body landmarks (like the elbow).
From a technical point of view, the vibrotactile bracelets are composed by cylindrical vibro-motors, independently controlled via an external PC using the Bluetooth communication protocol (see Fig. 1.4). The communication is realized with a RN42 Bluetooth module connected to an Arduino Pro Mini 3.3V with a baud rate of 9600. An Atmega 328 micro-controller installed on the Arduino board is used to independently control the vibration amplitude of each motor. The Precision Microdrives 303-100 Pico Vibe 3.2 mm vibration motors were placed into fabric pockets on the external surface of the bracelet (the width of the wristband is about 60 mm). The motors have a vibration frequency range of about 100-280 Hz (the maximal human sensitivity is achieved around 200 Hz-300 Hz [51]), typical normalized amplitude of 0.6 g, lag time of 21 ms, rise time of 32 ms and stop time of 35 ms. Note that the exploited motors are controlled by applying a certain amount of voltage which determines both frequency and amplitude. Thus, users feel changes in both the intensity and pitch of perception when frequency is varied.

1.2.7 Haptic feedback generation

In what follows, we illustrate our idea on how to convey motion information by using the proposed haptic devices. At first we present the haptic feedback mechanism from a high level point of view. It is worth noting that the proposed mechanism is general and independent from the two vibrotactile configurations described above. Then, we present how the haptic feedback policy is translated into vibrating stimuli for the two proposed

configurations.
Let us consider three stimuli, L (turn left), S (slow down) and R (turn right) and let $f_j(t)$ be the vibration frequency of stimulus $j \in \{L, S, R\}$ at time t. Let ΔT be the interval of time, $\hat{\omega}_h(t + \Delta T)$ is the predicted angular velocity of the user obtained by applying an Extended Kalman Filter (EKF) algorithm to the system defined by (1.1) and $\omega_h^*(t+\Delta T)$ represents the angular velocity computed by the controller in (1.5)-(1.6). Note that $\omega_h^*(t + \Delta T)$ is the angular velocity that the user should have at time $t + \Delta T$ in order to properly follow the robot. The proposed haptic feedback policy consists in sending a proper vibrotactile signal if the angular velocity $\omega_h^*(t+\Delta T)$ computed by the controller differs from the user's angular velocity $\hat{\omega}_h(t+\Delta T)$ more than a given threshold $\alpha \in \mathbb{R}^+$,

$$f_L(t) = 280 \text{ Hz, if } \omega_h^*(t + \Delta T) - \hat{\omega}_h(t + \Delta T) \geq \alpha,$$
$$f_R(t) = 280 \text{ Hz, if } \omega_h^*(t + \Delta T) - \hat{\omega}_h(t + \Delta T) \leq -\alpha.$$

The introduction of the threshold value α avoids to have unwanted and frequent oscillations in the human locomotion. The proposed feedback policy is based on the fact that the user smoothly rotates during the locomotion, thus the haptic feedback tries to direct the user toward the desired pose and then it stops when the user is close enough to it.
Since in real scenarios the maximal robot velocities are limited, it may happen that the robot can not maintain the formation if the human moves too fast, $v_r(t + \Delta T) > V_r$ (see Eq. (1.5)), where $V_r \in \mathbb{R}^+$ represents the maximal linear velocity of the robot. In this case, the robot is unable to maintain the formation and the user may collide with it. As a consequence, a proper signal is sent to warn the human if she/he is too close to the robot. Let $\delta \in \mathbb{R}^+$ the minimal human-robot distance, if $\|\mathbf{P}_r(t) - \mathbf{P}_h(t)\| < \delta$ then the user should slow down her/his pace,

$$f_S(t) = 280 \text{ Hz, if } \|\mathbf{P}_r(t) - \mathbf{P}_h(t)\| < \delta.$$

Note that the robot always tries to maintain the formation as long as $v_r(t + \Delta T) \leq V_r$. The human user is always free to decide her/his pace; only when the minimal human-robot distance is violated, a proper haptic signal is sent to the user in order to inform her/him to slow down her/his pace.
Concerning the configuration with a single bracelet, the three stimuli (L, S, R) are mapped one-to-one onto the three motors (left, center, right) of the bracelet. Concerning the bilateral configuration, vibration of the left wristband alerts the participant to turn left, and vice versa. While the *slow down* stimuli is displayed by a vibration of both bracelets. In order to reduce the *aftereffect* problem (Pacinian corpuscles that sense vibration on the skin may adapt to continuous stimuli, see [69] and the references therein) and to preserve users' ability to localize vibration, we command the tactor to be activated with a pulsed square wave, with period 2τ, $\tau \in \mathbb{R}^+$ and duty cycle of 50%. In other words, when a tactor is commanded, it vibrates at 280 Hz for τ s and then it is off for τs, cycling this behavior as long as needed by the algorithm. Concerning the bilateral configuration, when a bracelet is engaged its two vibrating motors alternatively vibrates in order to reduce the *aftereffect* problem while displaying the stimulus to the user. The vibrations of the tactors in each armband are regulated as for the tactors of the single-bracelet configuration, aforementioned described. However, the two pulsed square waves corresponding to the two tactors are in fact shifted of time τ. It is worth noting that, since two constraints may be violated at the same time (angular velocity and distance from the robot), two haptic stimuli should be presented at the same time. To keep the signals recognition as simple as possible, we do not consider superpositions of two signals, thus we present to the user the two stimuli in alternating order.

1.2.8 Evaluation of the haptic feedback

In this section we are not interested in exploring how humans perceive vibrational stimuli (in fact, an extensive psychophysical literature exists on this subject, see e.g. [24, 7, 30]), but rather in how the stimuli generated by the proposed bracelet are perceived by the subjects.

The proposed device has been tested on 7 healthy subjects (6 males, age range 23-40, 5 right-handed). None of the participants reported any deficiencies in the perception abilities (including vision, hearing, touch and proprioception). The participants signed informed consent forms. All of them were informed about the purpose of the experiment, were able to discontinue participation at any time, and no payment was provided for the participation.
Two different experiments were performed. The aim of the first test was to evaluate if unilateral and bilateral conditions can elicit the intended causal chain of stimulus-perception-decision. The second experiment was performed to evaluate the maximal stimuli duration that does not degrade the perception of the stimuli itself, since vibration effects may persist after the end of the stimulation (*aftereffect* problem). In order to evaluate the users experience, a questionnaire using bipolar Likert-type five-point scales was proposed to the subjects at the end of the experiments for both haptic conditions.
In the first experiment, participants were instructed to walk along a walkway whilst wearing the wristband/s and to react accordingly to the stimulus type (L, S, R) as soon as they perceived it. The length of the walkway was about 4 m. The vibrotactile stimulus was provided as soon as the user was 1.7 m in front of the obstacle. The bracelet/s continued to vibrate for 2 s. For each haptic configuration, each subject performed 12 trials (4 trials by three stimuli) organized in a pseudo-random order. All subjects were blindfolded and wore circumaural headphones reproducing white noise to mask distracting ambient or cuing sounds from the stimulators. Two RGB-D cameras tracked the motion of the human using a custom designed tracking algorithm (see Sec. 1.2.10). Sequences of stimulation appeared in short bursts with $\tau = 0.2$ s, vibrating frequency of 280 Hz and amplitude of 0.6 g. The vibration period 2τ was determined both by mechanical limitation of the proposed motors and by pilot studies conducted on a group of subjects in order to asses which interval they preferred. Such experiment allowed to evaluate the haptic devices in a scenario as similar as possible to the final setup.
In the second experiment, we analyzed if a signal with a long duration affected the perception of the signal itself (*aftereffect* problem). Each subject was comfortably seated at a desk. Both feedback conditions (unilateral and bilateral) were evaluated.
Circumaural headphones were worn, through which white noise was presented to mask distracting sounds. Each subject tested two sets of signals, each set was composed by pulsed signals with period $2\tau = 0.4$ s and 4 different durations (2 s, 10 s, 30 s and 60 s). The users did not know the duration of each signal. The signal was displayed to the bracelet and the user had to recognize when the bracelet stops to vibrate. For each signal we recorded the response time (interval of time between the end of the stimulus and the instant in which the user signaled the end of the vibrotactile signal). Responses were made by pressing a specific button on a keypad.
The questionnaire, consisting in 6 questions, was designed to evaluate their comfort, opinion of feedback quality, perceived effectiveness of the feedback, intrusiveness and flexibility of the device, and overall preferences. An answer of 5 meant *strongly agree*, whereas an answer of 1 meant *strongly disagree*.

1.2.9 Data analysis

In the first experiment, all subjects could correctly perceive the totality of the proposed stimuli for both haptic modalities. Fig. 1.5 presents an overhead view of. The average reaction time, i.e., the time between the onset of the haptic signals and the actual turning of the participants, was about 0.86 s ($\pm$0.13 of standard deviation) for unilateral configuration-left stimulus, 0.73 ($\pm$0.14) unilateral configuration-right stimulus, 0.87 ($\pm$0.16) unilateral configuration-stop stimulus, and 0.76 ($\pm$0.16) bilateral configuration-left stimulus, 0.80 ($\pm$0.14) bilateral configuration-right stimulus, and 0.73 ($\pm$0.14) bilateral configuration-stop stimulus. Comparison of the means among the feedback conditions was tested using a two-way repeated-measures ANOVA (ANalysis Of VAriance) [42]. ANOVA analyses the groups variances to test the heterogeneity of their means. Feedback conditions and localization of the feedback signals (L, S, R) were considered as within-subject factors. A family-wise level $\alpha_p = 0.05$ has been used for all tests. The collected data passed the Shapiro-Wilk normality test and the Mauchly's Test of Sphericity. The means did not differed significantly among feedback conditions

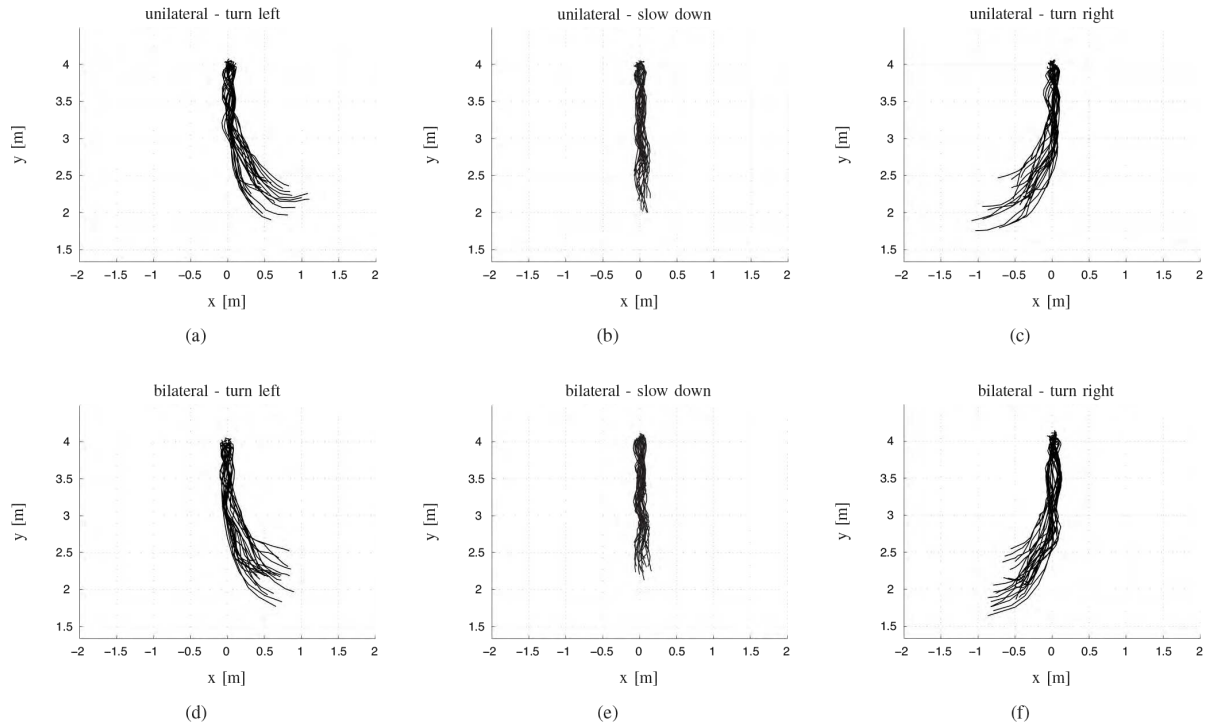

Figure 1.5: *Evaluation of the haptic feedback.* Trajectories performed by the users, as the participants walk from top to bottom using a single vibrotactile bracelet (a)-(c) and two bracelets (d)-(f), for the three stimuli (turn left, slow down and turn right), respectively.

$[F(1,6) = 3.905,\ p = 0.096,\ \alpha_p = 0.05]$, meaning that the reaction time of the users is not influenced by using the unilateral or bilateral condition to present directional cues. For each feedback condition, a one-way repeated measures ANOVA was conducted to determine whether reaction times for different stimuli (L, C, R) change in a significant way. In both conditions, the collected data passed the Shapiro-Wilk normality test and the Mauchly's Test of Sphericity. Tests showed that reaction times for the given stimuli do not depend on the type of stimulus: unilateral condition $[F(2,12) = 1.853,\ p = .199,\ \alpha_p = 0.05]$, bilateral condition $[F(2,12) = 0.154,\ p = .859,\ \alpha_p = 0.05]$.

It is worth pointing out that the time average response of the control signal incorporates the communication time between the computer and the bracelets and the activation time of the motors. The authors are aware that the proposed tests were conducted in a controlled environment and performed on healthy, able bodied adults and that the response time will increase in a real world situation, such as a loud factory or a busy hospital and with older/impaired subjects. Nevertheless, tests performed in Sec. 1.2.12 show the validity of our approach in a real scenario.

In the second experiment, we performed a one-way repeated-measures ANOVA on the perception time to determine whether reaction times for different stimulus durations (2 s, 10 s, 30 s, 60 s) are related to the duration of the stimulus itself. For both feedback conditions, the collected data passed the Shapiro-Wilk normality test and the Mauchly's Test of Sphericity. As a general result, participants recognized the end of the stimuli with mean delays of $[0.72 \pm 0.08,\ 0.70 \pm 0.19,\ 0.67 \pm 0.19,\ 0.78 \pm 0.12]$ s for the unilateral configuration and for the four durations, respectively, and of $[0.72 \pm 0.14,\ 0.75 \pm 0.14,\ 0.69 \pm 0.24,\ 0.79 \pm 0.14]$ for the bilateral configuration and for the four durations, respectively. Moreover, tests showed that delays in reacting to the

Questions	
U1	The unilateral condition is easy to use.
U2	The unilateral condition is not hampering.
U3	Following the cues of the unilateral condition is not tiring.
U4	Wearing one single bracelet is a comfortable solution.
U5	The cues suggested by the unilateral condition give comprehensive information for the guidance system.
U6	The cues suggested by the unilateral condition are easy to distinguish.
B1	The bilateral condition is easy to use.
B2	The bilateral condition is not hampering.
B3	Following the cues of the bilateral condition is not tiring.
B4	Wearing two bracelets is a comfortable solution.
B5	The cues suggested by the bilateral condition give comprehensive information for the guidance system.
B6	The cues suggested by the bilateral condition are easy to distinguish.

Table 1.1: Questionnaire proposed at the end of the experiments for the unilateral and bilateral condition, respectively.

Questions	mean	std	Questions	mean	std
U1	3.86	0.690	B1	4.00	0.816
U2	4.71	0.488	B2	4.29	0.488
U3	4.29	0.756	B3	4.14	0.690
U4	4.14	0.690	B4	2.86	0.690
U5	3.86	0.690	B5	3.71	0.756
U6	2.86	0.690	B6	4.29	0.756

Table 1.2: Results of the questionnaire for the unilateral and bilateral condition, respectively.

end of the stimulus do not depend on the duration of the stimulus: unilateral condition [$F(3, 18) = 0.610$, $p = 0.617$, $\alpha_p = 0.05$], bilateral condition [$F(3, 18) = .421$, $p = .740$, $\alpha_p = 0.05$]. Considering the similarity in time of the delays, we do think that they were not caused by the occurring of after-effect problems, but mainly from perception delays of the participants. Moreover, no tingling sensations were reported by the participants.

Survey responses

A questionnaire, presented in the form of bipolar Likert-type five-point scales (see Table 1.1), was proposed to the users in order to understand how they judged the two different feedback modalities. First four questions U1-4 and B1-4 investigated how much the users had found the two systems usable and comfortable, whereas questions U5-6 and B5-6 investigated if the users felt the suggested cue to be enough informative and if the cues were easy to distinguish in the two configurations. A series of Wilcoxon Signed-Rank tests was performed for highlighting statistical significance of the difference between the proposed questions (see Table 1.2). No significant differences have been found between question U1-3 and B1-3 and between question U5 and question B5, showing that the two systems are very easy to use, they are not tiring and do not hamper the user. Moreover, the haptic cues sent to the users have been found enough informative. Eventually, the unilateral solution have been found a comfortable solution [$Z = -2.251$, $p = 0.024$, $\alpha_p = 0.05$], whereas the cues sent though

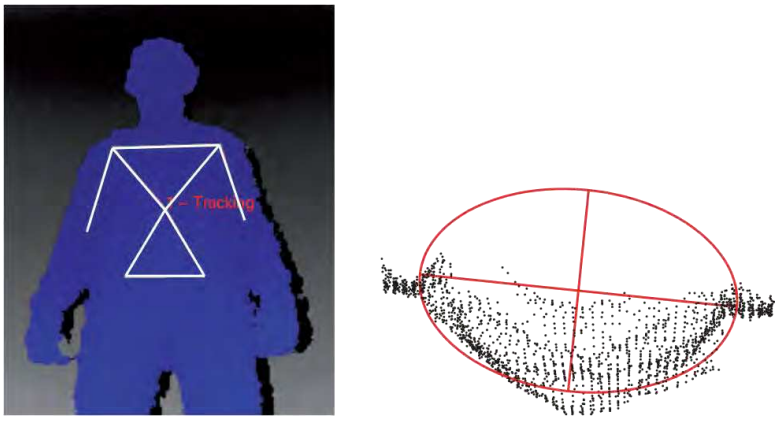

(a) (b)

Figure 1.6: *Human body tracking method on real data.* (a) NITE's skeleton tracker was used to initially detect the subject (the skeleton of the torso is shown in white). (b) Data points which were too far from the torso were removed, while the remaining points were down-sampled and expressed in the robot reference frame. The points were finally projected onto the robot xy-plane and the pose of the human body was detected via ellipse fitting.

the bilateral solution have been found easier to understand and more intuitive [$Z = -2.060$, $p = 0.039$, $\alpha_p = 0.05$].
Since the proposed feedback modalities are comparable (see also Sec. 1.2.9), in the experimental validation of the system we decided to use the bilateral configuration since cues sent through this solution have been found easier to understand. We believe that the results obtained in the experimental validation would have not differed too much if the unilateral condition was used.

1.2.10 Visual detection and tracking of the human

The controllers described in Sec. 1.2.4 need an estimation of the human's linear and angular velocities as well as her/his orientation with respect to the robot. This section provides an overview of the major steps of our method for detecting the human from the visual information provided by an RGB-D camera on-board the robot. We believe that our approach is relatively general and can be applied to other typologies of vision sensors (e.g., time-of-flight cameras) as well.
We used NITE skeleton tracker to initially detect and track the human (Fig. 1.6(a)) and the Point Cloud Library [53] to process the 3-D point data and extract the information about the human motion. Since the shoulders play an important role in the nonholonomic description of human locomotion (cf. [3]), in the detection phase we discarded all the 3-D points that were too far from the human's torso. We first down-sampled the data using a voxel grid filter with a leaf size of 1 cm. Then, we expressed the down-sampled point cloud in the robot reference frame and we projected the point cloud onto the robot xy-plane. Finally, an ellipse fitting [16] was performed over the points (Fig. 1.6(b)). In order to fully exploit the temporal information inherent to the human subject and to reliably estimate the human's velocities, in the proposed tracking algorithm we implemented an EKF algorithm [61] based on the position and orientation of the observed subject measured using the RGB-D camera. In case of failures of the skeleton tracker, we selected the 3-D points in the neighborhood of the predicted human pose. We projected such points onto the robot xy-plane, then we performed a cluster filtering discarding those clusters whose dimension was outside a given range and whose distance was far

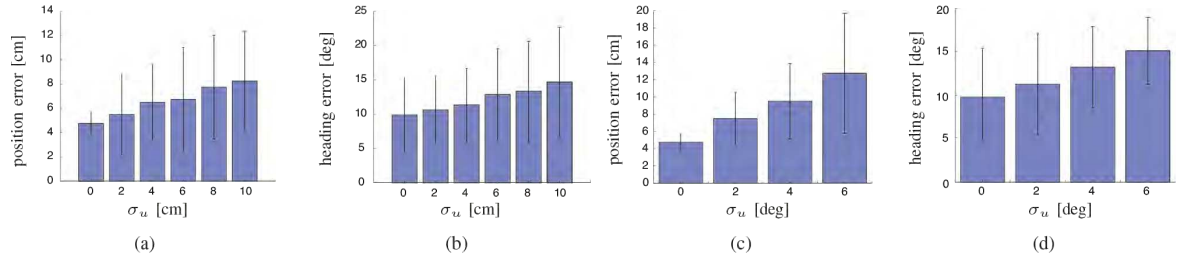

Figure 1.7: *Evaluation of the tracking algorithm.* Mean and standard deviation of the position and heading estimation error with increasing noise on: (a)-(b) depth estimation; (c)-(d) camera roll angle estimation. The noise was modeled as a Gaussian distribution centered in the actual value with variance σ_u.

enough from the last tracked human position. Finally, an ellipse fitting was performed over the resulting cluster. We considered the human body as the cluster that best fitted the ellipse, having the origin of the reference frame coincident with the ellipse center and orientation related to the ellipse's major axis. An example of this procedure is visible in the attached video.

1.2.11 Evaluation of the tracking algorithm

The proposed method runs at an average frame rate of 27 frames per second (FPS) on a laptop with 16 GB RAM, 2.4 GHz Intel i7 CPU, and NVIDIA GeForce GTX 765M graphic card. Synthetic data with ground truth information were used for the quantitative evaluation of the proposed method. This is a common approach in the relevant literature because ground truth data for real-world image sequences is hard to obtain. The employed synthetic sequence consisted of 7 trajectories, each one composed by 60 consecutive human poses (a total of 420 poses is considered) that encoded the human walking motion. All the trajectories lied in a 3 m $\times$ 3 m area. The user's heading ranged from -90 deg to 90 deg. Computer graphic was used to synthesize the required input for each considered pose. The method was also evaluated with respect to its tolerance to noisy observations. Two types of noise were considered: errors in depth estimation and errors in the camera orientation with respect to the floor since the proposed algorithm relies on the projection of the point cloud onto the robot xy-plane. We considered the camera calibration error as noise on the roll angle of the camera frame. We modeled the errors as a Gaussian distribution centered around the actual value with the variance controlling the amount of noise.
Let $(\tilde{x},\, \tilde{y},\, \tilde{\theta})^T$ be the estimated human pose. Figs. 1.7 (a)-(b) show the mean and the standard deviation of both the pose-estimation error $\|(x, y)^T - (\tilde{x}, \tilde{y})^T\|$ and the heading-estimation error $|\theta - \tilde{\theta}|$ when noise is added on depth estimation. Figs. 1.7 (c)-(d) show the mean and the standard deviation of both pose and heading-estimation error when noise is added on the estimation of the floor orientation with respect to the camera frame. From Fig. 1.7 we observe that the performance of our tracker is not critically affected by errors in depth estimation or in camera roll angle estimation.

1.2.12 Experimental validation

We tested the proposed control strategy (1.5) in an indoor environment using a Pioneer LX robot (with maximal linear velocity of 1.8 m/s) equipped with a backward facing Asus Xtion RGB-D camera (see Fig. 1.8).
Fifteen healthy subjects (age range 23-52, 12 males, 13 right-handed) were involved in our tests: five of them participated in the evaluation of the haptic bracelet (cf. Sec. 1.2.8). None of the participants reported any deficiencies in the perception abilities (including vision, hearing, touch and proprioception). The participants